

# Revisiting Model Stitching In the Foundation Model Era

Zheda Mai<sup>1,2,\*</sup>, Ke Zhang<sup>2</sup>, Fu-En Wang<sup>2</sup>, Zixiao Ken Wang<sup>2</sup>  
 Albert Y. C. Chen<sup>2</sup>, Lu Xia<sup>2</sup>, Min Sun<sup>2</sup>, Wei-Lun Chao<sup>1</sup>, Cheng-Hao Kuo<sup>2</sup>  
<sup>1</sup>The Ohio State University <sup>2</sup>Amazon

## Abstract

Model stitching, connecting early layers of one model (source) to later layers of another (target) via a light stitch layer, has served as a probe of representational compatibility. Prior work finds that models trained on the same dataset remain stitchable (negligible accuracy drop) despite different initializations or objectives. We revisit stitching for Vision Foundation Models (VFMs) that vary in objectives, data, and modality mix (e.g., CLIP, DINOv2, SigLIP 2) and ask: **Are heterogeneous VFMs stitchable?** We introduce a systematic protocol spanning the stitch points, stitch layer families, training losses, and downstream tasks. Three findings emerge. (1) *Stitch layer training matters:* conventional approaches that match the intermediate features at the stitch point or optimize the task loss end-to-end struggle to retain accuracy, especially at shallow stitch points. (2) *With a simple feature-matching loss at the target model’s penultimate layer, heterogeneous VFMs become reliably stitchable across vision tasks.* (3) *For deep stitch points, the stitched model can surpass either constituent model at only a small inference overhead (for the stitch layer).* Building on these findings, we further propose the VFM Stitch Tree (VST), which shares early layers across VFMs while retaining their later layers, yielding a controllable accuracy-latency trade-off for multimodal LLMs that often leverage multiple VFMs. Taken together, our study elevates stitching from a diagnostic probe to a practical recipe for integrating complementary VFM strengths and pinpointing where their representations align or diverge.

## 1. Introduction

The last decade has seen a shift from crafting bespoke model architectures to pre-training vision foundation models (VFMs)—typically Transformers—on massive, heterogeneous data with diverse objectives [3, 36, 48]. VFMs now serve as default backbones for many tasks thanks to strong generalization and transferability: users can often fine-tune

\*Work done during internship at Amazon.

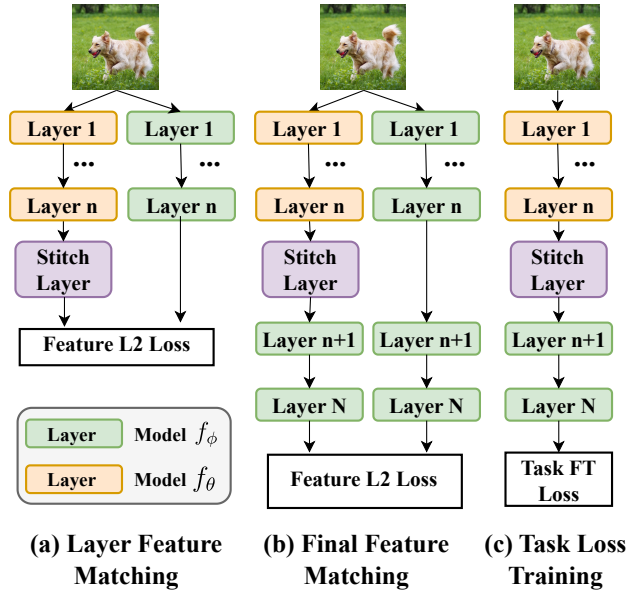


Figure 1. Model Stitching Training Strategies: (a) Layer Feature Matching trains the stitch layer to match features between the source and target models at the stitch point. (b) Final Feature Matching trains the stitch layer to match the final output features. (c) Task Loss Training optimizes the downstream objective directly.

with little (or no) task-specific data and reach accuracy that was out of reach only a few years ago.

A natural question follows. Although VFMs achieve different scores on downstream, capability-probing tasks [11, 42], are they fundamentally different “end-to-end,” or are their internal representations similar or compatible up to simple transformations? The answer matters for strategy: should we keep training new models (costly), or invest in managing and integrating existing ones?

We study this through model stitching: connecting the early layers of a source model to the later layers of a target model via a light stitch layer [2, 8] (Figure 1). Two models are stitchable if, with all original weights frozen and only the stitch layer trained, the stitched model matches the tar-

get model’s accuracy (*i.e.*, negligible drop). Existing results showed that small models (*e.g.*, ResNet-18 [14]) trained on the same dataset (*e.g.*, CIFAR-10 [27]) are stitchable despite different initializations or objectives. We extend this question to VFMs—large Transformers trained with different datasets (*e.g.*, LAION [20], WebLI [48], LVD-142M [33]), objectives (contrastive vs. reconstruction), and modality mixes (vision-language vs. pure vision)—including CLIP [36], DINOv2 [33], DINOv3 [33] and SigLIP 2 [48].

**Our contribution.** We develop a systematic protocol covering the stitch points, stitch layer designs, training losses, and multiple downstream tasks, and conduct a comprehensive analysis. Key insights are as follows.

**Naive stitching fails.** We revisit two common strategies to learn the stitch layer [2, 39]: 1) Layer Feature Matching—train the stitch layer to match features between the source and target models at the stitch point; and 2) Task-Loss Training—optimize only the downstream objective (*e.g.*, cross-entropy). In the VFM setting, both struggle, sometimes even much worse than either constituent model, and failures are more pronounced at shallow stitch points.

**Tailored training matters.** A closer look at the failure modes suggests that how to train the stitch layer matters. On the one hand, low feature matching error at the stitch points does not imply aligned final representations, particularly for shallow stitches. On the other hand, Task-Loss Training faces an intrinsic optimization challenge at shallow stitch points. As all target model’s layers after the stitch are frozen, gradients originating from the prediction head with weak supervision (*e.g.*, via the final pooled token) must traverse these frozen layers to adjust only the stitch layer, making the loss landscape poorly conditioned, especially when the stitch layer is randomly initialized. We therefore propose a simple two-stage recipe: (i) pre-train the stitch layer to match the target model’s final (pre-logit) patch features (Final Feature Matching), and then (ii) fine-tune with the downstream task loss. This Final Feature Matching dramatically reduces output-feature discrepancy, and the subsequent fine-tuning turns the good initialization into a strong stitched model accuracy—often matching or surpassing linear probes of either VFM across stitch points.

**Stitching integrates complementary strengths.** To ensure gains are not merely from adding stitch layer capacity, we insert the same trainable module into the source-only and target-only models. The stitched model consistently outperforms these self-stitched controls across stitch points (Figure 5), indicating that stitching VFMs is not only feasible but also has the potential to fuse complementarity between VFMs. We verify this across datasets and tasks—classification and semantic segmentation.

**From probe to system: VFM Stitch Tree (VST).** Modern multimodal systems (*e.g.* Multimodal LLMs and Vision-

Language Models) increasingly deploy multiple VFMs to capture complementary visual cues but incurs linear compute/memory overhead. Leveraging stitchability, we propose the VFM Stitch Tree (VST): share early layers across VFMs and retain specialized deep layers, enabling a controllable accuracy-latency trade-off. Taking a LLaVA model [30] with two VFMs as an example, VST with 22 shared layers and 1 specialized layer (4.3% extra resources) achieves 45% gain of the full two-VFM (requires 100% extra resources). With 14 shared + 9 specialized layers (40% extra), VST achieves 84% of the gain. Thus, VST offers a compute-aware knob for integrating complementary VFMs in multimodal systems.

**Summary.** Our paper has the following key contributions.

- We revisit model stitching for VFMs and show that with appropriate training, they are *reliably stitchable*. Across vision tasks, stitched models consistently improve upon baseline performance, suggesting complementary knowledge transfer between VFMs.
- Based on the findings, we propose VFM Stitch Tree, offering a controllable performance–efficiency trade-off for multimodal LLMs that employ multiple VFMs.
- To our knowledge, this is the first systematic study of model stitching for VFMs, aiming to advance this technique from a pure diagnostic probe toward a practical recipe and open a path for future work to integrate complementary VFM strengths.

## 2. Related Work

### 2.1. Model Stitching and Representational Analysis

**Foundations of Model Stitching.** Model stitching was first introduced by [28] as a method for understanding image representations by measuring their equivariance and equivalence. The core idea involves connecting layers from different models through a trainable transformation to assess representational compatibility. [2] extended this framework, demonstrating that models trained under similar conditions can be stitched together with minimal performance loss, leading to the influential “Anna Karenina hypothesis” that successful models learn similar internal representations.

**Functional vs. Structural Alignment.** The relationship between different notions of similarity has been critically examined in recent work. [8] introduced the crucial distinction between representational similarity (statistical measures on embeddings like CKA, CCA) and functional similarity (task performance compatibility), demonstrating that high representational similarity does not necessarily predict successful task transfer, and conversely, functional compatibility can exist with relatively low CKA values. This distinction is central to our work: while previous similarity measures assess statistical alignment, our self-stitching control directly evaluates functional knowledge fusion through

downstream task performance. [25] further surveyed these measures, highlighting the complexity of comparing neural network representations. Recent work by [39] challenged functional alignment interpretations, showing that models trained on entirely different tasks (ImageNet vs. birdsong recognition) or even with random clustered noise can be stitched successfully, arguing that stitching success primarily reflects representational clustering rather than semantic similarity. Our self-stitching control directly addresses these concerns by providing a rigorous baseline that isolates architectural effects from genuine knowledge fusion.

**Beyond Traditional Stitching.** [15] explored stitching between different layers and architectures, revealing unexpected compatibility patterns. [46] introduced techniques for merging task vectors from different models, while [47] proposed methods for dropping and rescaling parameters during model merging. [21] and [45] have also explored various approaches for combining multiple models, demonstrating growing interest in understanding how different models can be combined effectively.

## 2.2. Stitchable Architectures and Applications

Beyond using stitching for representation analysis, recent work has explored practical applications and architectures explicitly designed for stitchability.

**Training for Stitchability.** [35] introduced Stitchable Neural Networks (SN-Net), which are jointly trained to enable stitching across different model scales from a single training run, creating flexible model families for resource-adaptive inference. [34] extended this concept to Vision Transformers, demonstrating that stitching can enable efficient model compression and deployment across different ViT sizes. While these approaches focus on training models to be stitchable across scale variations, our work explores post-hoc stitching of independently trained VFMs with fundamentally different training paradigms (self-supervised vs. vision-language).

**Stitching Methodology.** [7] systematically compared direct matching (alignment using only representations) versus task loss matching (incorporating downstream task signals), demonstrating that task loss matching provides more robust performance and better captures functional similarity. Our approach follows this principle by combining layer-level feature mimicry for initialization with downstream task optimization for refinement, ensuring that stitched representations maintain task-relevant information while enabling cross-paradigm fusion.

**From Analysis to Fusion.** Traditional stitching work focused on assessing similarity through minimal performance degradation [2, 8]. Our work shifts this paradigm toward active knowledge fusion that improves performance, enabled by complementary specializations in heterogeneous VFMs rather than convergent representations in similar-condition

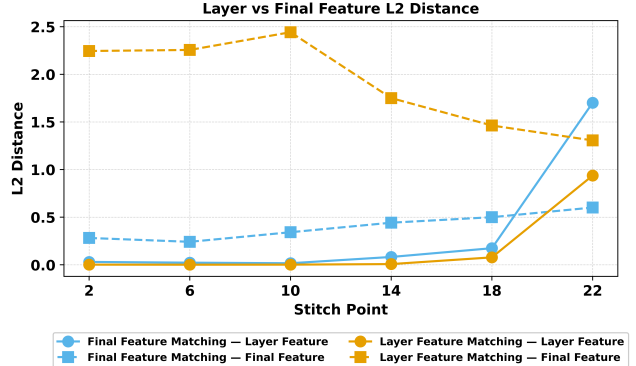


Figure 2. Layer Feature Matching vs. Final Feature Matching distance on SigLIP→DINOv2. Layer matching achieves low layer feature distance but high final feature distance, while final matching maintains low final feature distance.

models.

## 2.3. Vision Foundation Models

**Training Paradigms and Architectures.** Vision foundation models have emerged from diverse training paradigms. Self-supervised approaches like [33] learn visual representations without explicit supervision, while vision-language models like [36] and [48] leverage contrastive learning on image-text pairs. [40] and [9] have demonstrated the benefits of scaling both model size and training data.

**Complementary Specializations.** Different VFMs exhibit distinct strengths and weaknesses. [42] showed that vision-only models like DINOv2 excel at fine-grained visual pattern recognition, while vision-language models provide superior semantic grounding, motivating approaches that leverage multiple VFMs simultaneously.

**Model Combination and Ensemble Methods.** Recent work has explored various approaches for combining multiple foundation models. [45] and [21] have demonstrated improvements through model combination, supporting our findings about complementary specializations.

## 3. Model Stitching For VFMs

### 3.1. Problem Formulation

Let  $f = f^N \circ \dots \circ f^1$  be a VFM with  $N$  Transformer layers. For an image  $x$ , we define  $R_n$  as the function to map the input  $x$  to the intermediate features  $A^n \in \mathbb{R}^{d \times k}$  at layer  $n$ :  $R^n(x) = f^n \circ \dots \circ f^1(x) = A^n$ , where  $d$  and  $k$  denote the token dimension and number of token. Similarly, we define the function  $T^N$  that map the  $A^n$  to the output feature  $A^N$ :  $T^N(A^n) = f^N \circ \dots \circ f^n(A^n) = A^N$ .

Given a source and target VFM with parameters  $\theta$  and  $\phi$  respectively, we can stitch them at layer  $n$  by matching the source features  $A_\theta^n$  to the target feature  $A_\phi^n$  through a

trainable stitching layer  $S : \mathbb{R}^{d_\theta \times k} \rightarrow \mathbb{R}^{d_\phi \times k}$ . Thus, the stitched VFM can be represented by:

$$F(x) = T_\phi^N \circ S \circ R_\theta^n(x)$$

We want to emphasize that all the parameters in  $T_\phi^N$  and  $R_\theta^n$  are **frozen**; only the stitch layer  $S$  is trainable. Following [2, 8], for a given task, the source and target models are stitchable if the stitched model  $F$  has limited performance degradation compared to the target model  $f_\phi$ .

### 3.2. How To Train the Stitch Layer?

To answer whether heterogeneous VFMs are stitchable, we first explore fundamental question: *Are existing stitching approaches still effective for VFMs?* Two training strategies are most common (see Figure 1): (1) Layer Feature Matching [8] and (2) Task Loss Training [2]. In the following sections, we aim to conduct controlled experiments to evaluate their compatibility with VFM.

**Experiment Setup.** We start with two VFMs that are commonly used across domains: DINOv2-L [33] which is trained with only vision data (LVD-142M) in a self-supervised manner and SigLIP2-L [43], which is trained on vision-language data (WebLI) [5] with both vision self-supervised loss and language supervised loss. Both VFMs have 24 layers. In the following control studies, we choose a two-layer perceptron with ReLU (MLP) as the stitch layer since it’s a common feature projector for self-supervised learning [4] and multimodal LLM (e.g. LLaVA-1.5 [31]). We focus first on image classification with fMoW [6], a challenging and commonly used fine-tuning dataset for VFM evaluation [10]. More setup details are provided in the Appendix. Detailed investigation of stitch layer families, datasets, and tasks will be discussed in the latter sections.

#### 3.2.1. Layer Feature Matching (LFM)

The intuition behind LFM is that the target features should be easily matched from the source features if they are similar enough. Given unlabeled training images  $\mathcal{D} = \{x_i\}_{i=1}^M$ , LFM trains  $S$  by minimizing the feature discrepancy at layer  $n$ :

$$\mathcal{L}_{LFM} = \frac{1}{M} \sum_{i=1}^M \|S(R_\theta^n(x_i)) - R_\phi^n(x_i)\|_2^2$$

Note that LFM training is label-free, and if we pre-extract the source and target features, the training can be done without VFM inference.

**Observations.** To assess how well the target features can be transformed from source features across stitch points  $n \in [2, 6, 10, 14, 18, 22]$ , we measure on the validation set the mean  $\ell_2$  layer feature distance  $\|S(R_\theta^n(x)) - R_\phi^n(x)\|_2$  (●)

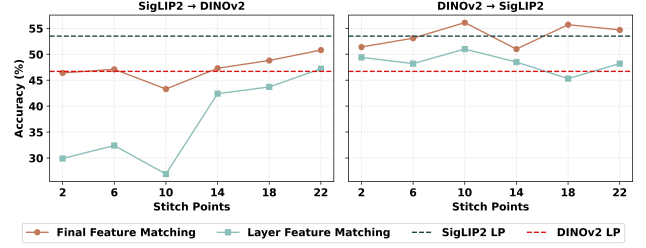


Figure 3. Final Feature Matching consistently shows better accuracy than Layer Feature Matching. In the DINOv2→SigLIP2 case, the stitched model can even exceed the performance of both constituent models.

in Figure 2). As expected, because LFM optimizes this directly, these distances are very small (order of  $10^{-3}$ ). However, small layer feature discrepancies do *not* guarantee similarity at the final features. On the contrary, we observe substantially larger final feature distances  $\|T_\phi^N(S(R_\theta^n(x))) - R_\phi^N(x)\|_2$  (■ in Figure 2), especially for shallow stitches. Intuitively, a small mismatch could accumulate and possibly be amplified by the frozen target layers, resulting in a pronounced final feature difference.

**Remedy.** Motivated by the observations above and inspired by feature distillation, we propose **Final Feature Matching** (FFM), which trains the stitch layer to directly match the final features at layer  $N$  between the stitch model  $F$  and target model  $f_\phi$ :

$$\mathcal{L}_{FFM} = \frac{1}{M} \sum_{i=1}^M \|T_\phi^N(S(R_\theta^n(x_i))) - T_\phi^N(R_\phi^n(x_i))\|_2^2$$

As shown in Figure 2, compared with LFM, FFM significantly reduces the final feature distances (■) at shallow stitch points—precisely where difference accumulation is most pronounced. More interestingly, although FFM directly matches the final features, it still retains similarly low layer feature distances (●) as LFM, suggesting that the supervision at the final layer can induce implicit local alignment at the stitch points. The better final feature alignment translates into better linear probing accuracy (Figure 3): stitch models trained with FFM consistently outperform their LFM counterparts across stitch points. Notably, in the DINOv2→SigLIP2 case, the stitched model can exceed the performance of both constituent models under linear probing, noting that same as LFM, FFM is label-free.

#### 3.2.2. Task Loss Training (TLT)

Task Loss Training (TLT) trains the stitching layer directly with downstream task loss using the labeled training data  $\mathcal{D} = \{(x_i, y_i)\}_{i=1}^M$ , where  $\ell$  is the task-specific loss (e.g.,

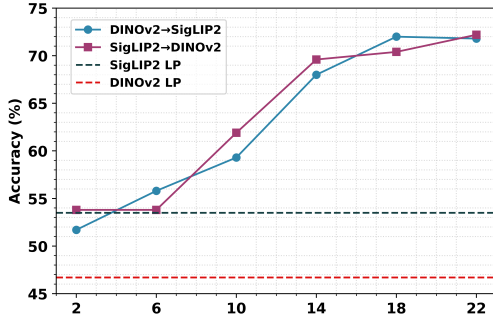


Figure 4. Our two stage training approach (Final Feature Matching + Task Loss Training) allows stitched models to consistently outperform linear-probing of both constituent models.

cross-entropy for classification):

$$\mathcal{L}_{task} = \frac{1}{M} \sum_{i=1}^M \ell(F(x_i), y_i) \quad (1)$$

**Observations.** Existing studies show that generally TLT outperform LFM across stitch points, as it directly optimizes the task objective. We also observe this pattern at deep stitch points. However, in contrast to existing observations, we find that TLT fails sharply for **shallow** stitches. Taking DINOv2→SigLIP2 stitching at layer 2 as an example, TLT attains only 25.1%, markedly below the linear probing for DINOv2 (46.7%), SigLIP2 (53.5%), LFM (49.4%) and FFM (51.4%).

**Remedy.** When stitching shallowly, all post-stitch target layers are frozen; thus, gradients from the prediction head must backpropagate through a long, fixed transformation to update *only* the stitch layer. This may attenuate update directions and cause optimization challenges, especially under random initialization and weak supervision (via pooled-token). To place the stitch layer in a better loss landscape, we adopt a simple two-stage procedure:

- (i) **Initialize** the stitch layer by pre-training with FFM
- (ii) **Fine-tune** the stitch layer with TLT

As summarized in Table 1, FFM initialization not only rescues naïve TLT at shallow stitches where TLT alone underperforms, but also yields consistent gains at deeper stitch points. In our experiments, it also significantly surpasses the linear-probing performance of both constituent models, as shown in Figure 4. We also observe that shallow layers consistently underperform. We hypothesize that early layers may encode pretraining-specific features (e.g., low-level visual features for DINOv2, text-aligned features for SigLIP2) while deep layers may develop more transferable, task-relevant representations, leading to easier stitching than shallow layers.

Our approach also resonates with a recent work [7] which argues that TLT can create out-of-distribution representations that optimize for task performance at the cost of representational fidelity. Our FFM initialization mitigates

Pre-train	DINOv2 → SigLIP2					
Layer	2	6	10	14	18	22
No FFM	25.1	39.4	52.6	62.3	68.6	68.6
FFM	<b>51.7</b>	<b>55.8</b>	<b>59.3</b>	<b>68.0</b>	<b>72.0</b>	<b>71.8</b>
Pre-train	SigLIP2 → DINOv2					
Layer	2	6	10	14	18	22
No FFM	38.7	<b>56.7</b>	58.3	64.4	70.4	70.1
FFM	<b>53.8</b>	53.8	<b>61.9</b>	<b>69.6</b>	<b>70.4</b>	<b>72.2</b>

Table 1. Final Feature Matching (FFM) initialization not only rescues naïve Task Loss Training at shallow stitches where it alone underperforms, but also yields consistent gains at deeper stitch points, showing the effectiveness of our two-stage approach. (Numbers are accuracy in %)

this risk by first preserving representational fidelity, then applying task-level adaptation for functionality.

## 4. Where Do Improvements Come From?

**Why do our results differ from prior works?.** With our two-stage training, the stitched model can substantially exceed linear probing for both the source and target (Figure 4). One might be tempted to conclude that VFMs are broadly stitchable, given that stitched models typically have around 0-10% accuracy drop compared to the target model in prior works [2]. However, in earlier studies, the source, target, and stitch layer were all trained/evaluated on the *same* dataset (e.g., CIFAR-10). In contrast, VFMs are pretrained on massive, diverse data and evaluated via fine-tuning on downstream data. Under this regime, improvements could arise simply from *task adaptation in the stitch layer*. We therefore design baselines that disentangle stitch layer capacity.

### 4.1. Self-Stitch Baseline

To rigorously test whether gains only stem from added capacity, we introduce a Self-Stitch baseline: inserting the identical stitch layer into the source-only and target-only models at the same stitch points. For example, for SigLIP2→DINOv2 stitched at layer 22, the baselines are SigLIP2→SigLIP2 and DINOv2→DINOv2 with an identical stitch module at layer 22. Self-stitch controls share the *same* trainable module, stitch point, training loss, and downstream data. Matching self-stitch performance therefore indicates *genuine VFM stitchability*.

### 4.2. Stitching integrates complementary strengths

Figure 5 compares the cross-VFM stitched model against their self-stitched baselines. Surprisingly, the stitched model consistently outperforms the self-stitched controls across stitch points, indicating that improvements are *not*

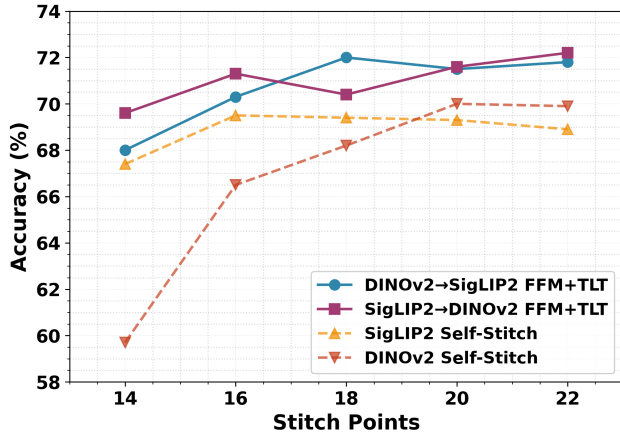


Figure 5. Stitched Model vs Self-Stitch. Both DINOv2→SigLIP2 and SigLIP2→DINOv2 (solid lines) consistently outperform their respective self-stitch baselines (dashed lines), demonstrating genuine knowledge fusion gains of +2.3% to +2.6% at optimal layers.

explained solely by stitch layer capacity or downstream fine-tuning. Instead, the results suggest that stitching heterogeneous VFMs is not only feasible but also has the potential to *fuse complementarity* between them.

## 5. Are Observations Consistent?

To stay focused on exploring *how to train the stitch layer* in previous sections, we adopt a fixed experiment setup. We assess the *consistency* of our findings across datasets, tasks, stitch-layer architectures, and VFMs.

### 5.1. Consistent Across Datasets & Tasks

In addition to fMoW [6] (satellite images), we evaluate on two widely used fine-grained classification datasets: iNaturalist-Subset [44] (animal species) and FGVC-Aircraft [32]. Beyond classification, we evaluate semantic segmentation on ADE20K [49, 50] with a linear decoder [23]. For simplicity in feature matching and to avoid confounding factors, we do not use any data augmentation during training.

As shown in Table 2, stitched models consistently surpass the corresponding self-stitch baselines across datasets in classification (+0.7% to +5.5%), indicating that the observed knowledge fusion gain is *not* a dataset-specific artifact but a generalizable observation. In ADE20K, we likewise observe steady improvements over self-stitching (+0.5 to +0.7 mIoU), demonstrating that complementary knowledge fusion extends to dense prediction. We hypothesize that DINOv2 contributes robust perceptual structure while SigLIP2 provides stronger semantic alignment; their combination, mediated by the stitch layer, yields modest yet reliable improvements.

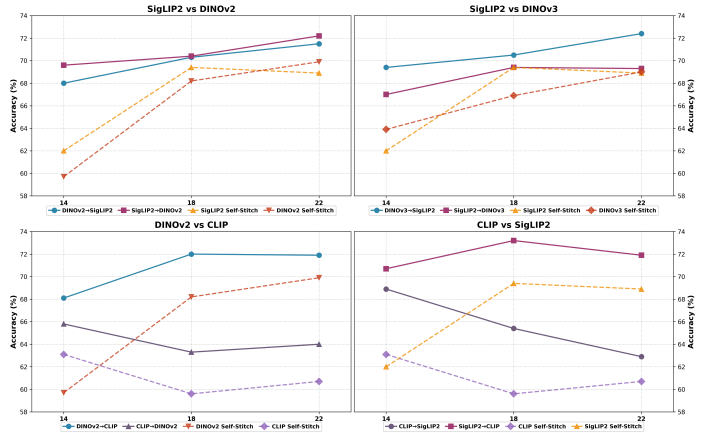


Figure 6. Evaluation of DINOv2, DINOv3, SigLIP2 and CLIP. The stitched models generally outperform both corresponding self-stitch baselines across stitched layers, except for using CLIP as the source model.

More dataset details, experiment setup and results are provided in the Appendix.

### 5.2. Validation Across More VFMs

Beyond the DINOv2 and SigLIP2 pairs, we further include the widely used CLIP and the recently released DINOv3 to verify the generality of our findings. As shown in Figure 6, the stitched models generally outperform both corresponding self-stitch baselines across stitched layers, except for using CLIP as the source model. In this case, CLIP is a weaker VFM in our setting (as evidenced by lower linear-probing and self-stitch performance), so the stitched model can improve over CLIP itself but still fails to match the stronger target model. Viewing the source as an encoder, this suggests that a weak encoder may discard task-critical information that the stronger target network cannot recover. Conversely, when CLIP serves as the target, the stitched model achieves strong performance, indicating that as long as a strong source model preserves rich intermediate representations, even a relatively weak target can still transform these features into high-quality final predictions. These results are reminiscent of observations in encoder–decoder architectures for detection and segmentation, where upgrading only the encoder/backbone (e.g., from ResNet-50 to ResNet-101) reliably improves performance, while substituting a strong backbone with a weaker one consistently degrades accuracy even under an unchanged decoder [16, 22, 29].

### 5.3. Stitch Layer: Linear, MLP, and LoRA

Beyond the default MLP, we explore two different stitch layers: (1) a linear layer and (2) source model’s  $n$  layer with LoRA [17], mapping  $(n-1)$ -layer features of the source to the  $n$ -layer features of the target. Concretely, (2) can be

Layer	Classification			Segmentation
	fMoW	iNaturalist	Aircraft	ADE20K
	6 / 14 / 22	6 / 14 / 22	6 / 14 / 22	14 / 22
DINOv2→DINOv2	41.5 / 59.7 / 69.9	56.9 / 81.5 / 91.2	37.8 / 79.3 / 91.2	35.4 / 50.9
SigLIP2→SigLIP2	50.5 / 62.0 / 68.9	71.2 / 88.5 / 87.3	67.9 / 88.1 / 89.3	44.5 / 50.5
DINOv2→SigLIP2	<b>55.8</b> / 68.0 / 71.8	75.9 / 89.1 / <b>92.8</b>	77.8 / 87.6 / <b>92.4</b>	44.9 / 51.2
SigLIP2→DINOv2	53.8 / <b>69.6</b> / <b>72.2</b>	<b>86.3</b> / <b>88.9</b> / 91.9	80.7 / 89.0 / 91.0	<b>49.0</b> / <b>51.4</b>

Table 2. Comprehensive results across all datasets and tasks. Classification results in accuracy (%), segmentation in mIoU (%). All results use the two-stage approach (Final Feature Matching + Task Loss Training).

Method	L2	L6	L10	L14	L18	L22	
D→S	Linear	26.1	54.3	<b>59.5</b>	66.5	69.1	69.6
	MLP	<b>51.7</b>	<b>55.8</b>	59.3	<b>68.0</b>	<b>72.0</b>	<b>71.8</b>
	LoRA	49.1	49.4	57.4	61.7	67.7	67.3
S→D	Linear	50.3	<b>56.4</b>	60.0	65.7	69.6	71.9
	MLP	<b>53.8</b>	53.8	61.9	<b>69.6</b>	<b>70.4</b>	<b>72.2</b>
	LoRA	48.3	56.2	<b>62.4</b>	65.3	66.2	65.0

Table 3. Stitch layer comparison: MLP consistently outperforms Linear and the LoRA option across stitching directions (D→S, S→D) where D and S denotes DINOv2 and SigLIP2 respectively.

represented as  $F_{LoRA}(x) = T_{\phi}^N \circ f_{(\theta, LoRA)}^n \circ R_{\theta}^{n-1}(x)$  where only LoRA parameters within  $f_{\theta, LoRA}^n$  are trainable. From a capacity perspective, the linear layer processes tokens independently and is the least expressive; the MLP adds nonlinearity while still operating per token; the LoRA option allows inter-token interactions and is the most expressive. As reported in Table 3, the MLP generally attains the strongest performance on the benchmarks considered, with linear trailing—as expected given its lower capacity. Somewhat counterintuitively, the LoRA-based option often underperforms the MLP despite its higher expressiveness. A plausible interpretation is that stitching may benefit from *controlled* mismatch that enables complementary information to be fused. If the stitch layer perfectly reproduces the target’s intermediate features,  $S(R_{\theta}^n(x)) = R_{\phi}^n(x)$ , the stitched model would be expected to match the target’s self-stitch, leaving little room for cross-model complementarity. We provide additional discussion in the Appendix.

#### Key Findings

- Heterogeneous VFMs trained with different data, objectives, and modalities remain stitchable across diverse vision tasks and datasets.
- Stitched VFMs consistently surpass self-stitch baselines, indicating that the gains aren’t only from the training of stitch layer but also the complementary strengths from VFMs.

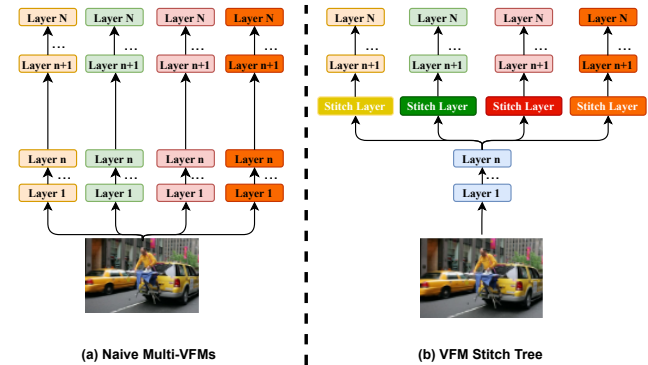


Figure 7. VFM Stitch Tree (VST) serves as a simple and efficient alternative to naively running all VFMs end-to-end.

## 6. From Insights To Applications

Our findings on VFM stitchability open a fertile space of research questions about knowledge fusion while also indicating clear potential for practical utility. We illustrate a concrete example by improving efficiency in multi-VFM multimodal settings.

### 6.1. The Efficiency Challenge For Multi-VFMs

Modern multimodal systems increasingly deploy multiple VFMs to capture complementary visual information. For example, MoF-LLaVA [42] combines CLIP and DINOv2 to preserve instruction following while improving visual grounding; OpenVLA [24] leverages SigLIP and DINOv2 to fuse low-level spatial structure with higher-level semantics; and Cambrian-1 [41] shows that assembling four VFMs with distinct strengths can lift MLLM performance across diverse benchmarks. However, there is no free lunch: with  $k$  VFMs, one must load all of them into GPU memory ( $k \times$ ) and process each input  $k$  times, yielding roughly  $k \times$  latency. **Question:** Can we design an architecture that retains the benefits of multiple VFMs *without* incurring linear compute and memory costs?

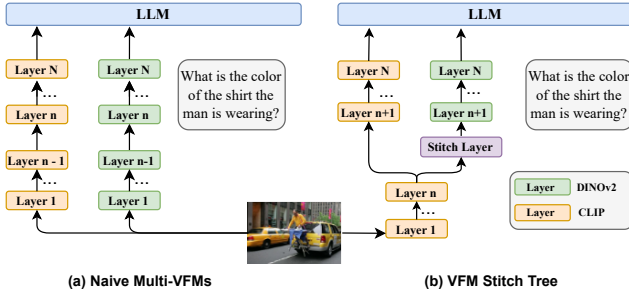


Figure 8. VFM Stitch Tree (VST) can be easily applied in various multimodal systems. This is an example of VST in a MoF-LLaVA with CLIP and DINOv2.

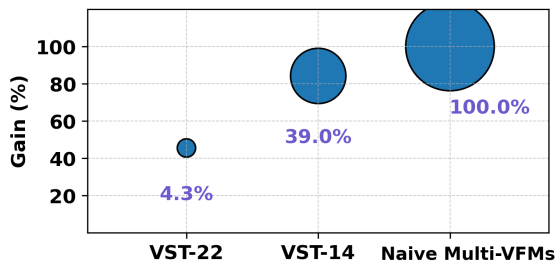


Figure 9. The performance–efficiency trade-offs for VST: VST can achieve 45% and 84% gain that requires 100% extra resources, with only 4.3% and 39% extra resources. We provide detailed gain numbers and resource calculation in the Appendix.

## 6.2. VFM Stitch Tree (VST)

Motivated by stitchability of VFMs, we propose the *VFM Stitch Tree (VST)*: shares common shallow layers across VFMs while *retains* model-specific deep layers, connected via stitch layers (Figure 7). VST serves as a simple and efficient alternative to naively running all VFMs end-to-end. Consider Cambrian-1 with four VFMs. A VST stitched at layer 14 reduces GPU memory and computation by 54% relative to running all four full VFMs (details in Appendix). We instantiate VST within a MoF-LLaVA (CLIP + DINOv2) with a Qwen-3B LLM [19]. The model is trained following the standard LLaVA-1.5 [31] training recipe and datasets. We evaluate VST stitched at layer 14 and 22, as demonstrated in Figure 8. Relative to a single-VFM LLaVA baseline, the naïve two-VFM MoF-LLaVA doubles backbone cost (100% extra). In contrast, our VST variants require only 39% (VST-14) and 4.3% (VST-22) additional resources. In this early exploration, we evaluate the MLLM on VQAv2 [13] and MME-Perception and MME-Cognition [12]. We provide experiments setup, detailed results and resource calculation in the Appendix.

As shown in Figure 9, VST-22, with just *one* additional specialized layer (4.3% overhead), recovers 45% of the two-VFM performance gain; when more budget is available, VST-14 reaches 84% of that gain at 39% overhead.

**Accuracy–efficiency knob.** Without VST, users face a binary choice: deploy an entire additional VFM (higher performance, 100% extra backbone cost) or none (no gain). VST introduces a *compute-aware knob* that interpolates between these extremes, enabling controllable performance–efficiency trade-offs under real deployment constraints. We view this as an initial step toward resource-conscious multi-VFM design; broader evaluations are provided in the Appendix.

## 6.3. Scope and Applications

VST is *one* concrete instantiation of how VFM stitching insights can be applied. The central takeaway is that heterogeneous VFMs can be stitched and fused to exploit complementary knowledge has potential applications across different domains and use cases. Potential applications include (1) dynamic VFM selection conditioned on input characteristics, (2) adaptive fusion for varying computational budgets, and (3) multi-task pipelines that require different VFM specializations, all leveraging the same underlying stitchability insight.

## 7. Conclusion

We revisited model stitching in the era of Vision Foundation Models and asked a simple but fundamental question: Are heterogeneous VFMs stitchable? Our systematic study across diverse objectives, datasets, and modality mixes shows that the answer is yes—provided that we train the stitch layer appropriately. We find that conventional strategies, such as matching intermediate activations at the stitch point or directly optimizing task loss, often fail to preserve accuracy, especially at shallow stitch points. In contrast, a simple feature-matching loss at the target model’s penultimate layer makes heterogeneous VFMs reliably stitchable across a range of vision tasks, with stitched models consistently improving over strong self-stitch baselines and revealing complementary knowledge transfer between VFMs.

Building on these empirical insights, we introduced the VFM Stitch Tree (VST), an architecture that shares early layers while retaining the later layers of multiple VFMs, enabling a controllable accuracy–latency trade-off for multimodal LLMs that rely on more than one visual encoder. Taken together, our results elevate stitching from a purely diagnostic tool to a practical recipe for integrating complementary VFM strengths and for pinpointing where their representations align or diverge. We hope this work provides both a blueprint and a testbed for future research on composing, reusing, and scaling VFMs within broader multimodal systems.

## References

- [1] Jinze Bai, Shuai Bai, Yunfei Chu, Zeyu Cui, Kai Dang, Xiaodong Deng, Yang Fan, Wenbin Ge, Yu Han, Fei Huang, et al. Qwen technical report. In *arXiv preprint arXiv:2309.16609*, 2023. 2
- [2] Yamini Bansal, Preetum Nakkiran, and Boaz Barak. Revisiting model stitching to compare neural representations. In *Advances in Neural Information Processing Systems (NeurIPS)*, 2021. 1, 2, 3, 4, 5
- [3] Mathilde Caron, Hugo Touvron, Ishan Misra, Hervé Jégou, Julien Mairal, Piotr Bojanowski, and Armand Joulin. Emerging properties in self-supervised vision transformers. In *Proceedings of the IEEE/CVF International Conference on Computer Vision (ICCV)*, pages 9650–9660, 2021. 1
- [4] Ting Chen, Simon Kornblith, Mohammad Norouzi, and Geoffrey Hinton. A simple framework for contrastive learning of visual representations. In *International conference on machine learning*, pages 1597–1607. PmlR, 2020. 4
- [5] Xi Chen, Xiao Wang, Soravit Changpinyo, Anthony J Piergiovanni, Piotr Padlewski, Daniel Salz, Sebastian Goodman, Adam Grycner, Basil Mustafa, Lucas Beyer, et al. Pali: A jointly-scaled multilingual language-image model. *arXiv preprint arXiv:2209.06794*, 2022. 4
- [6] Gordon Christie, Neil Fendley, James Wilson, and Ryan Mukherjee. Functional map of the world. *Proceedings of the IEEE Conference on Computer Vision and Pattern Recognition (CVPR)*, 2018. 4, 6, 1
- [7] Katherine M Collins, Umang Bhatt, and Adrian Weller. How not to stitch representations to measure similarity: Task loss matching versus direct matching. In *Proceedings of the AAAI Conference on Artificial Intelligence*, 2025. 3, 5
- [8] Adrián Csizsárik, Péter Kőrösi-Szabó, Ákos K. Matszangosz, Gergely Papp, and Dániel Varga. Similarity and matching of neural network representations. In *Advances in Neural Information Processing Systems (NeurIPS)*, pages 5656–5668, 2021. 1, 2, 3, 4
- [9] Alex Fang, Albin Madappally Jose, Amit Jain, Ludwig Schmidt, Alexander Toshev, and Vaishaal Shankar. Data filtering networks. *arXiv preprint arXiv:2309.17425*, 2023. 3
- [10] Enrico Fini, Mustafa Shukor, Xiujun Li, Philipp Dufter, Michal Klein, David Haldimann, Sai Aitharaju, Victor G Turrissi da Costa, Louis Béthune, Zhe Gan, et al. Multimodal autoregressive pre-training of large vision encoders. In *Proceedings of the Computer Vision and Pattern Recognition Conference*, pages 9641–9654, 2025. 4
- [11] Chaoyou Fu, Peixian Chen, Yunhang Shen, Yulei Qin, Mengdan Zhang, Xu Lin, Jinrui Yang, Xiawu Zheng, Ke Li, Xing Sun, et al. Mme: A comprehensive evaluation benchmark for multimodal large language models. In *arXiv preprint arXiv:2306.13394*, 2023. 1, 2
- [12] Chaoyou Fu, Peixian Chen, Yunhang Shen, Yulei Qin, Mengdan Zhang, Xu Lin, Jinrui Yang, Xiawu Zheng, Ke Li, Xing Sun, et al. Mme: A comprehensive evaluation benchmark for multimodal large language models. In *The Thirty-ninth Annual Conference on Neural Information Processing Systems Datasets and Benchmarks Track*, 2025. 8
- [13] Yash Goyal, Tejas Khot, Douglas Summers-Stay, Dhruv Batra, and Devi Parikh. Making the v in vqa matter: Elevating the role of image understanding in visual question answering. In *Proceedings of the IEEE conference on computer vision and pattern recognition*, pages 6904–6913, 2017. 8, 2
- [14] Kaiming He, Xiangyu Zhang, Shaoqing Ren, and Jian Sun. Deep residual learning for image recognition. In *Proceedings of the IEEE Conference on Computer Vision and Pattern Recognition (CVPR)*, pages 770–778, 2016. 2
- [15] Adam Hernandez, Rumén Dangovski, Peter Y Lu, and Marin Soljacic. Model stitching: Looking for functional similarity between representations. In *SVRHM 2022 Workshop @ NeurIPS*, 2022. 3
- [16] Xinyu Hou, Peng Chen, and Haishuo Gu. Lm-deeplabv3+: A lightweight image segmentation algorithm based on multi-scale feature interaction. *Applied Sciences*, 14(4):1558, 2024. 6
- [17] Edward J Hu, Yelong Shen, Phillip Wallis, Zeyuan Allen-Zhu, Yuanzhi Li, Shean Wang, Lu Wang, and Weizhu Chen. Lora: Low-rank adaptation of large language models. *arXiv preprint arXiv:2106.09685*, 10, 2021. 6
- [18] Drew A Hudson and Christopher D Manning. Gqa: A new dataset for real-world visual reasoning and compositional question answering. In *Proceedings of the IEEE/CVF conference on computer vision and pattern recognition*, pages 6700–6709, 2019. 2
- [19] Binyuan Hui, Jian Yang, Zeyu Cui, Jiayi Yang, Dayiheng Liu, Lei Zhang, Tianyu Liu, Jiajun Zhang, Bowen Yu, Keming Lu, et al. Qwen2. 5-coder technical report. *arXiv preprint arXiv:2409.12186*, 2024. 8
- [20] Gabriel Ilharco, Mitchell Wortsman, Ross Wightman, Cade Gordon, Nicholas Carlini, Rohan Taori, Achal Dave, Vaishaal Shankar, Hongseok Namkoong, John Miller, et al. Openclip. [https://github.com/mlfoundations/open\\_clip](https://github.com/mlfoundations/open_clip), 2021. 2
- [21] Gabriel Ilharco, Marco Tulio Ribeiro, Mitchell Wortsman, Suchin Gururangan, Ludwig Schmidt, Hannaneh Hajishirzi, and Ali Farhadi. Editing models with task arithmetic. In *International Conference on Learning Representations (ICLR)*, 2022. 3
- [22] Christoph Kamann and Carsten Rother. Benchmarking the robustness of semantic segmentation models. In *Proceedings of the IEEE/CVF Conference on Computer Vision and Pattern Recognition (CVPR)*, 2020. 6
- [23] Tommie Kerssies, Daan De Geus, and Gijs Dubbelman. How to benchmark vision foundation models for semantic segmentation? In *Proceedings of the IEEE/CVF Conference on Computer Vision and Pattern Recognition*, pages 1162–1171, 2024. 6, 2
- [24] Moo Jin Kim, Karl Pertsch, Siddharth Karamcheti, Ted Xiao, Ashwin Balakrishna, Suraj Nair, Rafael Rafailov, Ethan Foster, Grace Lam, Pannag Sanketi, et al. Openvla: An open-source vision-language-action model. *arXiv preprint arXiv:2406.09246*, 2024. 7
- [25] Max Klabunde, Tobias Schubert, and Sebastian Lapuschkin. Similarity of neural network models revisited: Measuring functional similarity. In *International Conference on Machine Learning (ICML)*, 2024. 3

- [26] Ranjay Krishna, Yuke Zhu, Oliver Groth, Justin Johnson, Kenji Hata, Joshua Kravitz, Stephanie Chen, Yannis Kalantidis, Li-Jia Li, David A Shamma, et al. Visual genome: Connecting language and vision using crowdsourced dense image annotations. *International journal of computer vision*, 123(1):32–73, 2017. 2
- [27] Alex Krizhevsky, Geoffrey Hinton, et al. Learning multiple layers of features from tiny images. 2009. 2
- [28] Karel Lenc and Andrea Vedaldi. Understanding image representations by measuring their equivariance and equivalence. In *Proceedings of the IEEE Conference on Computer Vision and Pattern Recognition (CVPR)*, 2015. 2
- [29] Tsung-Yi Lin, Piotr Dollár, Ross Girshick, Kaiming He, Bharath Hariharan, and Serge Belongie. Feature pyramid networks for object detection. In *Proceedings of the IEEE Conference on Computer Vision and Pattern Recognition (CVPR)*, pages 936–944, 2017. 6
- [30] Haotian Liu, Chunyuan Li, Qingyang Wu, and Yong Jae Lee. Visual instruction tuning. In *Advances in Neural Information Processing Systems (NeurIPS)*, 2023. 2
- [31] Haotian Liu, Chunyuan Li, Yong Jae Li, and Yong Jae Lee. Improved baselines with visual instruction tuning. *arXiv preprint arXiv:2310.03744*, 2024. 4, 8, 2
- [32] Subhransu Maji, Esa Rahtu, Juho Kannala, Matthew Blaschko, and Andrea Vedaldi. Fine-grained visual classification of aircraft. <http://www.robots.ox.ac.uk/~vgg/data/fgvc-aircraft/>, 2013. *arXiv preprint arXiv:1306.5151*. 6, 1
- [33] Maxime Oquab, Timothée Darcet, Théo Moutakanni, Huy V Vo, Marc Szafraniec, Vasil Khalidov, Pierre Fernandez, Daniel Haziza, Francisco Massa, Alaaeldin El-Nouby, et al. Dinov2: Learning robust visual features without supervision. *arXiv preprint arXiv:2304.07193*, 2023. 2, 3, 4, 1
- [34] Zizheng Pan, Jianfei Cai, and Bohan Zhuang. Stitched vits are flexible vision backbones. *arXiv preprint arXiv:2307.06304*, 2023. 3
- [35] Zizheng Pan, Bohan Zhuang, Haoyu He, Jing Liu, and Jianfei Cai. Stitchable neural networks. In *Proceedings of the IEEE/CVF Conference on Computer Vision and Pattern Recognition (CVPR)*, pages 16041–16050, 2023. 3
- [36] Alec Radford, Jong Wook Kim, Chris Hallacy, Aditya Ramesh, Gabriel Goh, Sandhini Agarwal, Girish Sastry, Amanda Askell, Pamela Mishkin, Jack Clark, et al. Learning transferable visual models from natural language supervision. In *Proceedings of the 38th International Conference on Machine Learning (ICML)*, 2021. 1, 2, 3
- [37] Oriane Siméoni, Huy V. Vo, Maximilian Seitzer, Federico Baldassarre, Maxime Oquab, Cijo Jose, Vasil Khalidov, Marc Szafraniec, Seungeun Yi, Michaël Ramamonjisoa, Francisco Massa, Daniel Haziza, Luca Wehrstedt, Jianyuan Wang, Timothée Darcet, Théo Moutakanni, Leonel Sentana, Claire Roberts, John Brandt, Camille Couprie, Julien Mairal, Hervé Jégou, Patrick Labatut, and Piotr Bojanowski. Dinov3. *arXiv preprint arXiv:2508.10104*, 2025. 1
- [38] Amanpreet Singh, Vivek Natarajan, Meet Shah, Yu Jiang, Xinlei Chen, Dhruv Batra, Devi Parikh, and Marcus Rohrbach. Towards vqa models that can read. In *Proceedings of the IEEE/CVF conference on computer vision and pattern recognition*, pages 8317–8326, 2019. 2
- [39] Damian Smith, Harvey Mannerling, and Antonia Marcu. Functional alignment can mislead: Examining model stitching. In *Proceedings of the 42nd International Conference on Machine Learning (ICML)*, 2025. 2, 3
- [40] Quan Sun, Yuxin Fang, Ledell Wu, Xinlong Wang, and Yue Cao. Eva-clip: Improved training techniques for clip at scale. *arXiv preprint arXiv:2303.15389*, 2023. 3
- [41] Peter Tong, Ellis Brown, Penghao Wu, Sanghyun Woo, Adithya Jairam Vedagiri IYER, Sai Charitha Akula, Shusheng Yang, Jihan Yang, Manoj Middepogu, Ziteng Wang, et al. Cambrian-1: A fully open, vision-centric exploration of multimodal llms. *Advances in Neural Information Processing Systems*, 37:87310–87356, 2024. 7, 4
- [42] Shengbang Tong, Zhuang Liu, Yuexiang Zhai, Yi Ma, Yann LeCun, and Saining Xie. Eyes wide shut? exploring the visual shortcomings of multimodal llms. *arXiv preprint arXiv:2401.06209*, 2024. 1, 3, 7, 2
- [43] Michael Tschannen, Alexey Gritsenko, Xiao Wang, Muhammad Ferjad Naeem, Ibrahim Alabdulmohsin, Nikhil Parthasarathy, Talfan Evans, Lucas Beyer, Ye Xia, Basil Mustafa, et al. Siglip 2: Multilingual vision-language encoders with improved semantic understanding, localization, and dense features. *arXiv preprint arXiv:2502.14786*, 2025. 4, 1
- [44] Grant Van Horn, Oisín Mac Aodha, Yang Song, Yin Cui, Chen Sun, Alex Shepard, Hartwig Adam, Pietro Perona, and Serge Belongie. The inaturalist species classification and detection dataset. In *Proceedings of the IEEE Conference on Computer Vision and Pattern Recognition (CVPR)*, pages 8769–8778, 2018. 6, 1
- [45] Mitchell Wortsman, Gabriel Ilharco, Samir Yitzhak Gadre, Rebecca Roelofs, Raphael Gontijo-Lopes, Ari S Morcos, Hongseok Namkoong, Ali Farhadi, Yair Carmon, Simon Kornblith, et al. Model soups: Averaging weights of multiple fine-tuned models improves accuracy without increasing inference time. In *International Conference on Machine Learning (ICML)*, pages 23965–23998, 2022. 3
- [46] Prateek Yadav, Derek Tam, Leshem Choshen, Colin Raffel, and Mohit Bansal. Ties-merging: Resolving interference when merging models. In *Advances in Neural Information Processing Systems (NeurIPS)*, 2023. 3
- [47] Le Yu, Bowen Xiang, Haiyang Jiang, et al. Dare: Drop and rescale for better model merging. In *International Conference on Learning Representations (ICLR)*, 2024. 3
- [48] Xiaohua Zhai, Basil Mustafa, Alexander Kolesnikov, and Lucas Beyer. Sigmoid loss for language-image pre-training. *arXiv preprint arXiv:2303.15343*, 2023. 1, 2, 3
- [49] Bolei Zhou, Hang Zhao, Xavier Puig, Sanja Fidler, Adela Barriuso, and Antonio Torralba. Scene parsing through ade20k dataset. In *Proceedings of the IEEE Conference on Computer Vision and Pattern Vision (CVPR)*, 2017. 6, 1
- [50] Bolei Zhou, Hang Zhao, Xavier Puig, Tete Xiao, Sanja Fidler, Adela Barriuso, and Antonio Torralba. Semantic understanding of scenes through the ade20k dataset. In *International Journal of Computer Vision*, 2019. 6, 1

- [51] Baichuan Zhou, Ying Hu, Xi Weng, Junlong Jia, Jie Luo, Xien Liu, Ji Wu, and Lei Huang. Tynyllava: A framework of small-scale large multimodal models. *arXiv preprint arXiv:2402.14289*, 2024. [2](#)

# Revisiting Model Stitching In the Foundation Model Era

## Supplementary Material

We provide details omitted in the paper.

- Sec. A: Experiment and dataset details
- Sec. B.1: Detailed results

### A. Experiment and Dataset Details

#### A.1. Vision Foundation Models (VFMs)

We use the following VFMs in our experiments.

- **DINOv2-L** [33]: A ViT-L/14 encoder trained with self-supervised DINOv2 on a curated collection of  $\sim 142\text{M}$  internet images, using a teacher–student distillation objective that encourages consistency across multi-crop image views without labels. In our experiments, we feed  $336 \times 336$  inputs with patch size 14.
- **CLIP-L** [36]: A ViT-L/14 vision encoder from CLIP, trained jointly with a text encoder on  $\sim 400\text{M}$  image–text pairs from the web using a contrastive objective that pulls matched image–caption pairs together and pushes mismatched pairs apart in a shared embedding space. We use the vision tower with  $336 \times 336$  inputs and patch size 14.
- **SigLIP2-L** [43]: A ViT-L/16 multilingual vision–language encoder trained on a diverse mixture of web image–text data with a sigmoid-based image–text matching loss, augmented with captioning-style pretraining, self-distillation, masked prediction, and online data curation to improve dense features and localization. We use  $384 \times 384$  inputs and patch size 16.
- **DINOv3-L** [37]: A ViT-L/16 self-supervised encoder from the DINOv3 family, trained at large scale on a multi-domain image collection with a distillation-style objective and Gram anchoring to stabilize dense feature maps, yielding strong frozen representations for both global and dense tasks. In our experiments, we use  $384 \times 384$  inputs and patch size 16.

#### A.2. Fine-Grained Classification

##### A.2.1. Dataset Details

**fMoW** [6] The Functional Map of the World (fMoW) dataset is a commonly used and challenging dataset for VFM evaluation. It is a collection of high-quality remote-sensing satellite images collected worldwide, annotated with 62 land-use and functional categories (e.g., airfield, port, hospital). We use the fMoW-RGB variant, which provides pan-sharpened RGB crops and associated metadata. Since the original dataset is highly imbalanced, we construct a class-balanced subset with 230 training and 26 test images per class (14,260 train / 1,612 test) so that our study

can focus on model stitching itself rather than confounding effects from label imbalance, which would complicate the interpretation of stitching behavior.

**iNaturalist-Subset** [44] The iNaturalist 2021 dataset family has become a standard testbed for assessing VFM performance on fine-grained, real-world biodiversity recognition. It is a large-scale and heavily imbalanced species classification benchmark that reflects naturally occurring long-tailed distributions. To obtain a controlled yet challenging setting for analyzing stitching, we sample 106 species from three visually similar Lepidoptera families (Sphingidae, Pieridae, Pyralidae) and rebalance the data with 200 training and 50 test images per class (21,200 train / 5,300 test). This balanced construction removes imbalance as an additional variable, enabling a cleaner analysis of how stitching choices impact performance.

**FGVC-Aircraft** [32] FGVC-Aircraft is widely adopted as a canonical fine-grained classification benchmark for VFMs. The version we use contains 102 aircraft models and approximately 10k images, with each model appearing in around 100 images. We follow the standard split with 6.6k training and 3.3k test images, which requires distinguishing subtle variations in shape, livery, and viewpoint.

##### A.2.2. Training Details

For all fine-grained classification experiments, we adopt linear probing: a single linear classifier is trained on pooled image features while all VFM parameters remain frozen.

For *layer feature matching*, we first extract intermediate features from both source and target VFMs and train the stitch MLP purely on these features; no additional VFM forward passes are required during this phase. For *final feature matching*, we extract features from the target model and train only the stitch layer.

To isolate the effect of stitching, we do not apply any data augmentation. We use the AdamW optimizer in all experiments, train for up to 100 epochs with early stopping (patience of 5 epochs), and tune the learning rate in  $\{0.001, 0.005, 0.01\}$ . For layer feature matching, we use a batch size of 256; all other configurations use a batch size of 128. Training is performed with automatic mixed precision using `bfloat16`.

##### A.2.3. Semantic Segmentation

##### A.2.4. Dataset Details

**ADE20K** [49, 50] ADE20K is a scene-centric semantic segmentation dataset with pixel-level annotations for

150 object and stuff categories across diverse indoor and outdoor environments. We adopt the canonical split with 20,210 training images and 3,000 held-out test images. The dense annotations cover scenes, objects, and parts, making ADE20K a challenging benchmark for evaluating dense prediction performance.

### A.2.5. Training Details

For semantic segmentation, we train a linear layer to predict per-pixel class logits for each patch token. The linear layer produces a low-resolution logit map (e.g.,  $24 \times 24$  for a model with patch size 14 and  $336 \times 336$  input), which is then bilinearly upsampled to the original image resolution to obtain the final segmentation map.

For layer feature matching and final feature matching, we reuse the optimization and hyperparameter settings described for classification (optimizer, learning rates, batch sizes, early stopping, and mixed precision). All remaining experimental details for segmentation follow [23].

## A.3. VFM Stitch Tree for Multimodal LLM

### A.3.1. Dataset Details

We use the LLaVA-1.5 training data prepared by TinyLLaVA.<sup>1</sup> LLaVA-1.5-Pretrain (PT) consists of 558k image-caption pairs [31], while LLaVA-1.5-SFT comprises 665k visual instruction-tuning conversations that combine academic-style VQA [13, 18, 26, 38] samples with instruction-tuning data from LLaVA-Instruct [30]. In our preliminary study, we evaluate on VQA-v2 [13] and MME [11].

### A.3.2. Training Details

We jointly use LLaVA-1.5-Pretrain and LLaVA-1.5-SFT to train the stitch layer for one epoch with a learning rate of 0.001 and batch size 64. All remaining hyperparameters follow the TinyLLaVA recipe [51]. We adopt Qwen2.5-3B [1] as the LLM and employ an interleaved mixture-of-features (MoF) [42] strategy when combining visual tokens from CLIP and DINOv2.

## B. Detailed and Additional Results

### B.1. Self-Stitch

To rigorously test whether gains only stem from added capacity, we introduce a Self-Stitch baseline: inserting the identical stitch layer into the source-only and target-only models at the same stitch points. Fig. 10 illustrates the difference between model stitching and self-stitching baseline.

<sup>1</sup>We use the data preparation pipeline from TinyLLaVA: <https://tinylava-factory.readthedocs.io/en/latest/Prepare%20Datasets.html>

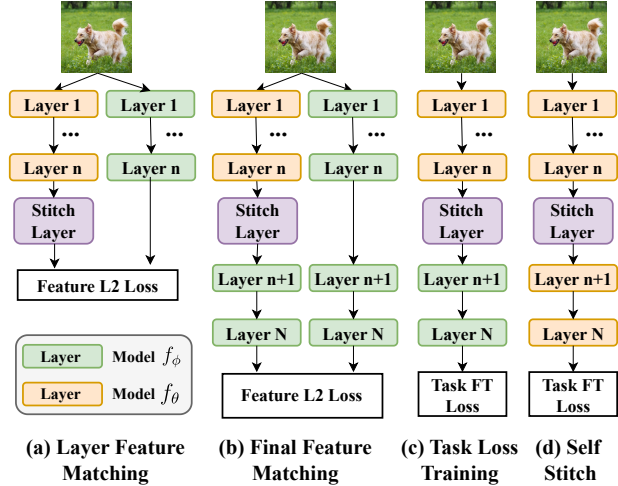


Figure 10. Model Stitching Training Strategies: (a) Layer Feature Matching trains the stitch layer to match features between the source and target models at the stitch point. (b) Final Feature Matching trains the stitch layer to match the final output features. (c) Task Loss Training optimizes the downstream objective directly. (d) Self-Stitch inserts the stitch layer to the source-only and target-only models at the same stitch points.

## B.2. Layer and Final Feature Matching

We present a detailed comparison between Layer and Final Feature Matching in Tab. 4. We observe that Final Feature Matching consistently outperforms Layer Feature Matching across all configurations. Notably, in the DINOv2  $\rightarrow$  SigLIP2 setting, the stitched model surpasses the performance of both constituent models. Our results further indicate that stitching a lower-performing source model to a higher-performing target is more effective than the reverse; DINOv2  $\rightarrow$  SigLIP2 consistently achieves higher accuracy than SigLIP2  $\rightarrow$  DINOv2, regardless of the matching strategy employed.

## B.3. Stitching Between Different VFMs

To verify the generality of our findings, we extend our analysis beyond DINOv2 and SigLIP2 to include the widely adopted CLIP and the recently released DINOv3. Detailed comparisons between Stitched models, Self-Stitch baselines, and Linear Probing are provided in Tabs. 5 to 9. Consistent with our previous results, stitched models generally outperform their corresponding self-stitch baselines across most layers. The primary exception arises when CLIP is utilized as the source model; we discuss the potential causes for this phenomenon in the main paper.

## B.4. Prediction Analysis

To better understand how knowledge fusion affects prediction behavior, we compare each stitched model (DINOv2  $\rightarrow$  SigLIP2 and SigLIP2  $\rightarrow$  DINOv2) against

	DINOv2		SigLIP2			
Linear Probing	46.7		53.5			
Layer	2	6	10	14	18	22
<b>Layer Feature Matching</b>						
DINOv2 → SigLIP2	49.4	48.2	51.0	48.5	45.3	48.2
SigLIP2 → DINOv2	29.9	32.4	26.9	42.4	43.7	47.2
<b>Final Feature Matching</b>						
DINOv2 → SigLIP2	51.4	53.1	56.1	51.0	55.7	54.7
SigLIP2 → DINOv2	46.4	47.1	43.3	47.3	48.8	50.8

Table 4. **Comparison of Layer and Final Feature Matching.** We report linear probing accuracy for different stitching strategies. **Orange** indicates performance surpassing the SigLIP2 baseline, while **Blue** indicates performance surpassing the DINOv2 baseline.

	DINOv2		CLIP	
Linear Probing	46.7		46.4	
Layer	6	14	18	22
DINOv2 → DINOv2	41.5	59.7	68.2	69.9
CLIP → CLIP	48.5	63.1	59.6	60.7
CLIP → DINOv2	53.1	65.8	63.3	64.0
DINOv2 → CLIP	<b>54.1</b>	<b>68.1</b>	<b>72.0</b>	<b>71.9</b>

Table 5. Stitched Model vs Self-Stitch vs Linear Probing: DINOv2 and CLIP.

	DINOv2		SigLIP2	
Linear Probing	46.7		53.5	
Layer	6	14	18	22
DINOv2 → DINOv2	41.5	59.7	68.2	69.9
SigLIP2 → SigLIP2	50.5	62.0	69.4	68.9
SigLIP2 → DINOv2	53.8	<b>69.6</b>	70.4	<b>72.2</b>
DINOv2 → SigLIP2	<b>55.8</b>	68.0	<b>72.0</b>	71.8

Table 6. Stitched Model vs Self-Stitch vs Linear Probing: DINOv2 and SigLIP2.

the two self-stitched baselines (DINOv2→DINOv2 and SigLIP2→SigLIP2) on fMoW and iNaturalist. We discard trivial cases where all three models are correct or all three are wrong, and partition the remaining examples into the scenarios in Tab. 10:

1. **Preserve (Cols. 1–2).** At least one self-stitched model is correct and the stitched model is also correct, preserving the correct prediction.
2. **Rescue (Col. 3).** Both self-stitched models are wrong but the stitched model is correct.
3. **Interference (Cols. 4–6).** At least one self-stitched

	SigLIP2		CLIP	
Linear Probing	53.5		46.4	
Layer	6	14	18	22
SigLIP2 → SigLIP2	50.5	62.0	69.4	68.9
CLIP → CLIP	48.5	63.1	59.6	60.7
CLIP → SigLIP2	48.3	68.9	65.4	62.9
SigLIP2 → CLIP	<b>59.8</b>	<b>70.7</b>	<b>73.2</b>	<b>71.9</b>

Table 7. Stitched Model vs Self-Stitch vs Linear Probing: SigLIP2 and CLIP.

	DINOv3		SigLIP2	
Linear Probing	50.0		53.5	
Layer	6	14	18	22
DINOv3 → DINOv3	44.7	63.9	66.9	69.0
SigLIP2 → SigLIP2	50.5	62.0	69.4	68.9
SigLIP2 → DINOv3	<b>58.6</b>	67.0	69.4	69.3
DINOv3 → SigLIP2	45.0	<b>69.4</b>	<b>70.5</b>	<b>72.4</b>

Table 8. Stitched Model vs Self-Stitch vs Linear Probing: DINOv3 and SigLIP2.

	DINOv2		DINOv3	
Linear Probing	46.7		50.0	
Layer	6	14	18	22
DINOv2 → DINOv2	41.5	59.7	68.2	69.9
DINOv3 → DINOv3	44.7	63.9	66.9	69.0
DINOv3 → DINOv2	43.8	<b>67.2</b>	67.9	<b>72.0</b>
DINOv2 → DINOv3	<b>57.8</b>	65.0	<b>69.2</b>	70.3

Table 9. Stitched Model vs Self-Stitch vs Linear Probing: DINOv2 and DINOv3.

model is correct but the stitched model becomes wrong.

Across both datasets and stitch directions, the total count of *preserve* and *rescue* scenarios clearly exceeds that of *interference* scenarios, indicating that the stitched models benefit more from fusing complementary signals than they suffer from conflicts between the two backbones.

We further ask whose behavior the stitched model tends to follow when the two self-stitched models disagree. On fMoW, where the two self-stitched accuracies are similar, the stitched models are more likely to match the *source* model: for SigLIP2→DINOv2, the number of cases where the stitched prediction agrees with SigLIP2→SigLIP2 substantially exceeds the cases where it agrees with DINOv2→DINOv2, and an analogous trend holds for DINOv2→SigLIP2. In contrast, on iNaturalist, where DINOv2→DINOv2 is the stronger self-stitched model, both stitch directions tend to align with the stronger model’s predictions regardless of whether it is used as

### fMoW

	Scenario						Acc.		Scenario						Acc.
DINOv2→DINOv2	W	R	W	R	R	W	69.9	DINOv2→DINOv2	W	R	W	R	R	W	69.9
SigLIP2→SigLIP2	R	W	W	R	W	R	68.9	SigLIP2→SigLIP2	R	W	W	R	W	R	68.9
<b>SigLIP2→DINOv2</b>	R	R	R	W	W	W	72.2	<b>DINOv2→SigLIP2</b>	R	R	R	W	W	W	71.8
Count	116	78	47	40	86	33		Count	77	116	54	52	48	72	

### iNaturalist

	Scenario						Acc.		Scenario						Acc.
DINOv2→DINOv2	W	R	W	R	R	W	91.2	DINOv2→DINOv2	W	R	W	R	R	W	91.2
SigLIP2→SigLIP2	R	W	W	R	W	R	87.3	SigLIP2→SigLIP2	R	W	W	R	W	R	87.3
<b>SigLIP2→DINOv2</b>	R	R	R	W	W	W	91.9	<b>DINOv2→SigLIP2</b>	R	R	R	W	W	W	92.8
Count	138	292	75	68	116	53		Count	127	331	80	49	77	64	

Table 10. Analysis of Predictions: **R** and **W** denote Right and Wrong predictions for each model, with counts in the last row and accuracies in the last column for fMoW and iNaturalist. Stitched models fall into complementarity scenarios (stitched is correct while at least one self-stitched baseline is wrong) far more often than interference ones (stitched is wrong while at least one self-stitched baseline is correct). When the two self-stitched models disagree, the stitched model tends to follow the source model on fMoW but follows the stronger model DINOv2 on iNaturalist.

source or target.

Overall, these analyses support our interpretation that stitching primarily acts as a knowledge-fusion mechanism: it preserves or rescues correct predictions from at least one backbone much more often than it disrupts them, and when there is a strong/weak asymmetry, the stitched model gravitates toward the stronger expert’s decisions.

## B.5. VFM Stitch Tree (VST) for Multimodal LLM (MLLM)

### B.5.1. Computation Comparison

Table 11 compares the computational cost of running all VFMs independently (Full) versus our VST method at various stitch points. We illustrate the efficiency gains using Cambrian-1 with 4 VFMs [41]. Assuming a standard 24-layer ViT-L architecture [43], and noting that MLLMs typically extract features from the second last layer (layer 23) [31], we base our calculations on a 23-layer depth. While the “Full” setting incurs a 300% computational overhead compared to a single VFM, VST-14 significantly reduces this burden. By sharing the first 14 layers and maintaining specialized branches only from layer 15 onwards, VST-14 requires processing only  $3 \times (23 - 14) = 27$  additional layers. This results in an overhead of just  $27/23 \approx 117\%$ , demonstrating a substantial efficiency improvement over the independent baseline.

## B.6. VST as an Accuracy-Efficiency Knob

We introduce the concept of “Normalized Gain” to quantify the effectiveness of VST relative to running all VFMs inde-

Number of VFMs	Full	VST-6	VST-14	VST-22
2	100%	74%	39%	4%
3	200%	148%	78%	9%
4	300%	222%	117%	13%
5	400%	296%	156%	17%

Table 11. **Comparison of Additional Computation Cost.** We report the additional increase in computation compared to a single VFM. “Full” denotes running all VFMs independently. “VST- $n$ ” denotes a shared backbone up to the stitch point  $n$ , where layers 1 through  $n$  are shared and subsequent layers are executed independently. For example, VST-14 shares the first 14 layers and maintains specialized branches from layer 15 onwards.

pendently. Table 12 provides the step-by-step derivation of these values for both VST-22 and VST-14.

We define the Normalized Gain as the ratio between the performance improvement achieved by VST ( $\Delta_{\text{VST}}$ ) and the maximum improvement achieved by running all VFMs independently ( $\Delta_{\text{max}}$ ):

$$\text{Normalized Gain (\%)} = \frac{\Delta_{\text{VST}}}{\Delta_{\text{max}}} = \frac{\text{Perf}_{\text{VST}} - \text{Perf}_{\text{CLIP}}}{\text{Perf}_{\text{Full}} - \text{Perf}_{\text{CLIP}}} \quad (2)$$

As illustrated in Tab. 12:

- The **Orange Row** represents the **Denominator** ( $\Delta_{\text{max}}$ ): the total performance gap between the single-model baseline and the computationally expensive naive full running (100% additional cost).
- The **Pink Rows** represent the **Numerator** ( $\Delta_{\text{VST}}$ ): the actual gain realized by our VST method.

Model Configuration	VQAv2			MME		Efficiency Metrics	
	Yes/No	Number	Other	Percep.	Cogn.	Avg Gain %	Add. Cost
<b>1. Define the Upper Bound (Denominator)</b>							
(A) CLIP Baseline	91.75	58.74	69.00	1418.5	277.1	-	0%
(B) Full (CLIP + DINOv2)	92.72	61.64	70.30	1460.3	311.8	-	100%
<b>(C) Max Gain (<math>\Delta_{\max} = B - A</math>)</b>	<b>0.97</b>	<b>2.90</b>	<b>1.30</b>	<b>41.8</b>	<b>34.7</b>	<b>(Denom.)</b>	<b>-</b>
<b>2. VST-22: The Lightweight Knob (High Efficiency)</b>							
(D) VST-22 (Ours)	92.12	59.21	69.15	1451.6	305.7	-	4.3%
<b>(E) VST Gain (<math>\Delta_{\text{VST}} = D - A</math>)</b>	<b>0.37</b>	<b>0.47</b>	<b>0.15</b>	<b>33.1</b>	<b>28.6</b>	<b>(Num.)</b>	<b>-</b>
<b>Normalized Gain (<math>\% = E/C</math>)</b>	<b>38.1%</b>	<b>16.2%</b>	<b>11.5%</b>	<b>79.1%</b>	<b>82.5%</b>	<b>45.5%</b>	<b>4.3%</b>
<b>3. VST-14: The Balanced Knob (High Performance)</b>							
(F) VST-14 (Ours)	92.54	60.69	69.88	1474.4	301.8	-	39.0%
<b>(G) VST Gain (<math>\Delta_{\text{VST}} = F - A</math>)</b>	<b>0.79</b>	<b>1.95</b>	<b>0.88</b>	<b>55.9</b>	<b>24.7</b>	<b>(Num.)</b>	<b>-</b>
<b>Normalized Gain (<math>\% = G/C</math>)</b>	<b>81.4%</b>	<b>67.2%</b>	<b>67.7%</b>	<b>133.7%</b>	<b>71.1%</b>	<b>84.2%</b>	<b>39.0%</b>

Table 12. **Detailed Calculation of Normalized Gain.** Comparison of the “Lightweight” VST-22 and the “Balanced” VST-14. The **Orange Row** represents the gain ( $\Delta_{\max}$ ) achieved by the computationally expensive Naive ensemble (100% Cost). The **Pink Rows** represent the actual gain ( $\Delta_{\text{VST}}$ ) achieved by our method. The **Normalized Gain** is calculated as  $\Delta_{\text{VST}}/\Delta_{\max}$ . Note that VST-22 achieves nearly half the total gain (45.5%) with negligible cost (4.3%).

The results highlight the versatility of VST as a compute-aware knob. **VST-22** serves as an ultra-lightweight option, recovering **45.5%** of the total possible gain while incurring a negligible **4.3%** increase in backbone cost. Conversely, **VST-14** acts as a balanced high-performance option, recovering **84.2%** of the total gain for only **39%** of the additional cost. This granular control allows practitioners to maximize model utility within specific computational budgets.

Consequently, we view VST as a vital *accuracy–efficiency knob* for architecture design. Without VST, practitioners face a rigid binary choice: either deploy an entire additional VFM (yielding higher performance but incurring **100%** extra backbone cost) or deploy none (yielding no gain). VST transforms this discrete step function into a continuous spectrum. By serving as a compute-aware knob, our method effectively interpolates between these extremes, enabling controllable performance–efficiency trade-offs that can be dynamically tuned to meet strict real-world deployment constraints.